Preclinical Evaluation of ^{18}F-Labeled Anti-HER2 Nanobody Conjugates for Imaging HER2 Receptor Expression by Immuno-PET

Ganesan Vaidyanathan[1], Darryl McDougald[1], Jaeyeon Choi[1], Eftychia Koumarianou[1], Douglas Weitzel[2], Takuya Osada[3], H. Kim Lyerly[3], and Michael R. Zalutsky[1]

[1]*Department of Radiology, Duke University Medical Center, Durham, North Carolina;* [2]*Department of Radiation Oncology and Cancer Biology, Duke University Medical Center, Durham, North Carolina; and* [3]*Department of Surgery, Duke University Medical Center, Durham, North Carolina*

The human growth factor receptor type 2 (HER2) is overexpressed in breast as well as other types of cancer. Immuno-PET, a noninvasive imaging procedure that could assess HER2 status in both primary and metastatic lesions simultaneously, could be a valuable tool for optimizing application of HER2-targeted therapies in individual patients. Herein, we have evaluated the tumor-targeting potential of the 5F7 anti-HER2 Nanobody (single-domain antibody fragment; ~13 kDa) after ^{18}F labeling by 2 methods. **Methods:** The 5F7 Nanobody was labeled with ^{18}F using the novel residualizing label *N*-succinimidyl 3-((4-(4-^{18}F-fluorobutyl)-1H-1,2,3-triazol-1-yl)methyl)-5-(guanidinomethyl)benzoate (^{18}F-SFBTMGMB; ^{18}F-RL-I) and also via the most commonly used ^{18}F protein–labeling prosthetic agent *N*-succinimidyl 3-^{18}F-fluorobenzoate (^{18}F-SFB). For comparison, 5F7 Nanobody was also labeled using the residualizing radioiodination agent *N*-succinimidyl 4-guanidinomethyl-3-^{125}I-iodobenzoate (^{125}I-SGMIB). Paired-label (^{18}F/^{125}I) internalization assays and biodistribution studies were performed on HER2-expressing BT474M1 breast carcinoma cells and in mice with BT474M1 subcutaneous xenografts, respectively. Small-animal PET/CT imaging of 5F7 Nanobody labeled using ^{18}F-RL-I also was performed. **Results:** Internalization assays indicated that intracellularly retained radioactivity for ^{18}F-RL-I-5F7 was similar to that for coincubated ^{125}I-SGMIB-5F7, whereas that for ^{18}F-SFB-5F7 was lower than coincubated ^{125}I-SGMIB-5F7 and decreased with time. BT474M1 tumor uptake of ^{18}F-RL-I-5F7 was 28.97 ± 3.88 percentage injected dose per gram of tissue (%ID/g) at 1 h and 36.28 ± 14.10 %ID/g at 2 h, reduced by more than 90% on blocking with trastuzumab, indicating HER2 specificity of uptake, and was also 26%–28% higher ($P < 0.05$) than that of ^{18}F-SFB-5F7. At 2 h, the tumor-to-blood ratio for ^{18}F-RL-I-5F7 (47.4 ± 13.1) was significantly higher ($P < 0.05$) than for ^{18}F-SFB-5F7 (25.4 ± 10.3); however, kidney uptake was 28–36-fold higher for ^{18}F-RL-I-5F7. **Conclusion:** ^{18}F-RL-I-5F7 is a promising tracer for evaluating HER2 status by immuno-PET; however, in settings in which renal background is problematic, strategies for reducing its kidney uptake may be needed.

Key Words: HER2; Nanobody; ^{18}F; immuno-PET; residualizing label

J Nucl Med 2016; 57:967–973
DOI: 10.2967/jnumed.115.171306

Despite the introduction of molecularly targeted therapies, death rates in women from breast cancer remain higher than those from any other malignancy except lung cancer (*1,2*). Because the human epidermal growth factor receptor type 2 (HER2, ErbB2/*neu*) is associated with tumor aggressiveness and poor prognosis, a variety of HER2-targeted therapies have been developed (*3*). A notable example is trastuzumab, a monoclonal antibody reactive with the extracellular domain of HER2, which can significantly increase survival in 25%–30% of breast cancer patients with HER2-positive disease. As with other molecularly targeted therapies, those directed against HER2 are largely ineffective in patients who are HER2-negative at the time of treatment. Moreover, those patients not likely to benefit would be needlessly subjected to treatment-related side effects such as the cardiotoxicity associated with trastuzumab treatment (*4*), which could be avoided if their HER2 status was known. Thus, it is imperative to assess the HER2 levels in tumors of individual patients before administering trastuzumab or other HER2-targeted therapy. Indeed, evaluation of HER2 expression in every primary breast cancer has been recommended by both the American Society of Clinical Oncology and the European Group of Tumor Markers (*5,6*).

The 2 primary techniques for assaying HER2 levels, immunohistochemical staining and fluorescence in situ hybridization (*7*), are problematic because they are invasive and may not be representative because of heterogeneous HER2 expression within the primary tumor. Moreover, they are not informative about differences in HER2 levels between primary lesion and metastases or among different metastatic sites (*8–10*), leading to recommendations that a biopsy be obtained to evaluate target status in metastases before selecting an appropriate therapy (*11*). This need has provided motivation for the evaluation of HER2-specific antibodies, antibody fragments, and Affibody molecules labeled with positron emitters for assessment of global HER2 expression by immuno-PET (*12–14*).

Herein, we explore the feasibility of utilizing ^{18}F-labeled Nanobodies as probes for evaluating HER2 status by immuno-PET. Nanobodies (a.k.a. VHH; 12–15 kDa) are antigen-binding fragments

Received Dec. 14, 2015; revision accepted Feb. 3, 2016.
For correspondence or reprints contact: Ganesan Vaidyanathan, Box 3808, Department of Radiology, Duke University Medical Center, Durham, NC 27710.
E-mail: ganesan.v@duke.edu
Published online Feb. 18, 2016.

of heavy-chain-only antibodies from *Camelidae* (*15,16*) having biologic half-lives (1–2 h) that are ideal for labeling with ^{18}F (1.8 h). Our ^{18}F-labeling strategy is based on our previous studies with radioiodine labeling of the anti-HER2 Nanobody 5F7 using the residualizing label *N*-succinimidyl 4-guanidinomethyl-3-*I-iodobenzoate (*I-SGMIB) (*16*). The *I-SGMIB-5F7 conjugate exhibited substantially higher uptake in HER2-expressing xenografts than those reported previously for any combination of Nanobody, radionuclide, and tumor model. Herein, the 5F7 Nanobody was labeled with ^{18}F using an agent conceptually analogous to *I-SGMIB, *N*-succinimidyl 3-((4-(4-^{18}F-fluorobutyl)-1H-1,2,3-triazol-1-yl)methyl)-5-(guanidinomethyl)benzoate (^{18}F-SFBTMGMB; ^{18}F-RL-I) (Fig. 1) (*17*), and with ^{18}F-SFB (*18*), and then evaluated in HER2-positive BT474M1 breast carcinoma cells and xenograft models.

MATERIALS AND METHODS

Nanobody, Cells, and Culture Conditions

The production, purification, and characteristics of anti-HER2 5F7 Nanobody, obtained from Ablynx, in the format lacking the GlyCysCys tail, have been described previously (*19*). HER2-expressing BT474M1 human breast carcinoma cells (*20*) were cultured in Dulbecco modified Eagle medium/F12 medium containing 10% fetal calf serum, streptomycin (100 μg/mL), and penicillin (100 IU/mL) (Sigma Aldrich). Cells were cultured at 37°C in a humidified incubator under 5% CO_2 with medium changed every 2 d. When about 80% confluent, cells were subcultured by trypsinization (0.05% Trypsin-ethylenediaminetetraacetic acid).

Radiolabeling Nanobody 5F7

Details of the synthesis of ^{18}F-RL-I-5F7, ^{18}F-SFB-5F7, and ^{125}I-SGMIB-5F7, as well as the affinity and immunoreactivity of these immunoconjugates, have been reported in a recent publication (*17*) (the supplemental materials provide additional synthetic details [supplemental materials are available at http://jnm.snmjournals.org]).

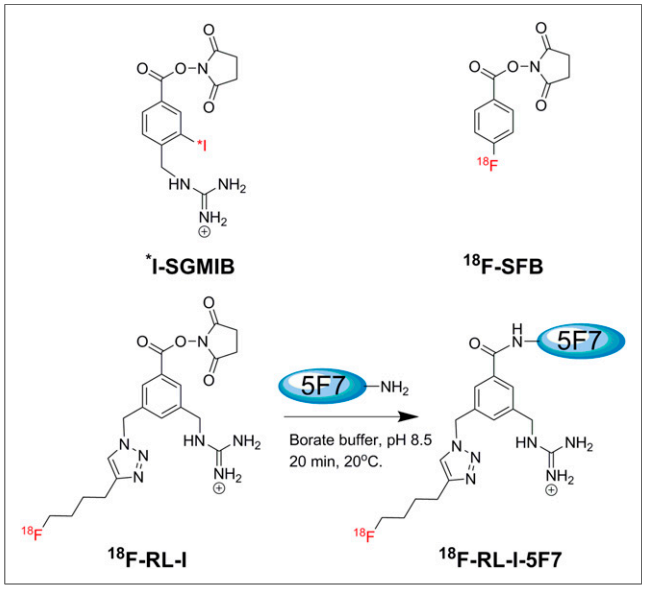

FIGURE 1. Structures of *I-SGMIB and ^{18}F-SFB and scheme for labeling 5F7 Nanobody using ^{18}F-RL-I.

Internalization Assays

Two sets of internalization assays were performed on BT474M1 cells comparing the behavior of ^{18}F-RL-I-5F7 or ^{18}F-SFB-5F7 with coincubated ^{125}I-SGMIB-5F7 as described previously (*19*) but only at 1, 2, and 4 h (details are provided in the supplemental materials).

Biodistribution Studies

Paired-label studies were performed in mice with BT474M1 subcutaneous xenografts (details are provided in the supplemental materials) following protocols approved by the Duke University Institutional Animal Care & Use Committee (*16,19*). In experiment 1, 2 groups of 5 mice were injected via the tail vein with 148 kBq (4 μCi; 0.9 μg) of ^{125}I-SGMIB-5F7 and 370 kBq (10 μCi; 5.9 μg) of ^{18}F-RL-I-5F7 in 100 μL of phosphate-buffered saline. In experiment 2, 2 groups of 5 mice received 148 kBq (4 μCi; 0. 5 μg) of ^{125}I-SGMIB-5F7 and 555 kBq (15 μCi; 3.8 μg) of ^{18}F-SFB-5F7. At 1 and 2 h after injection, 5 mice were killed with an overdose of isoflurane and dissected, and tissues and blood were harvested. Tissues, blood, and urine were weighed and counted for ^{125}I and ^{18}F activity in an automated γ-counter. From these data, percentage injected dose per gram of tissue (%ID/g) and tumor–to–normal-tissue ratios were calculated.

Small-Animal PET/CT Imaging

Imaging was performed on an Inveon microPET/CT system (Siemens) in groups of 4 mice with BT474M1 xenografts with and without HER2 blocking. For HER2 blocking, mice were injected intravenously with trastuzumab in phosphate buffer (4.4 mg in 200 μL; 220 mg/kg) 24 h before injection of 3.0–4.5 MBq (80–120 μCi; ~10 μg) of ^{18}F-RL-I-5F7 in 100 μL of phosphate-buffered saline. Mice were anesthetized using 2%–3% isoflurane in oxygen and placed prone in the scanner gantry for a 5-min PET acquisition followed by a 5-min CT scan. Control mice were imaged at 1 and 2 h while HER2-blocked mice were imaged at 1 h. List-mode PET data were histogram-processed and the images reconstructed using standard 3-dimensional ordered-subset expectation maximization/maximum a posteriori algorithm—two 3-dimensional ordered-subset expectation maximization iterations, and eighteen maximum a posteriori iterations—with a cutoff (Nyquist) of 0.5. Images were corrected for attenuation (CT-based) and radioactive decay. Image analysis was performed using Inveon Research Workplace software (Siemens). Regions of interest were drawn around tumors on the coregistered PET and CT images, and ^{18}F uptake was expressed as SUV and %ID/g.

Statistical Analysis

Results are presented as mean ± SD. The statistical significance of differences in uptake between 2 tracers that were coinjected (^{18}F vs. ^{125}I) was calculated with a 2-tailed, paired Student *t* test using Microsoft Excel, whereas a 2-tailed unpaired Student *t* test was used to compare the results obtained for the 2 ^{18}F-labeling methods in different groups of animals. A *P* value of less than 0.05 was considered statistically significant.

RESULTS

Internalization Assays

In the first study (Fig. 2A), intracellularly trapped ^{18}F-RL-I-5F7 activity was 49.3% ± 1.6%, 49.9% ± 2.1%, and 47.5% ± 2.1%, of initially cell-bound levels, at 1, 2, and 4 h, respectively, values that were slightly lower than those for coincubated ^{125}I-SGMIB-5F7 (53.4% ± 0.8%, 55.0% ± 1.2%, and 52.1% ± 0.3%, respectively). In contrast, intracellular counts from ^{18}F-SFB-5F7 decreased from 39.9% ± 0.3% at 1 h to 24.5% ± 1.1% at 4 h (Fig. 2B), values that were significantly lower ($P < 0.05$) than those for coincubated ^{125}I-SGMIB-5F7 (1 h, 51.2% ± 0.7%; 4 h, 51.3% ± 2.6%). Normalizing to coadministered ^{125}I-SGMIB-5F7 was performed for the

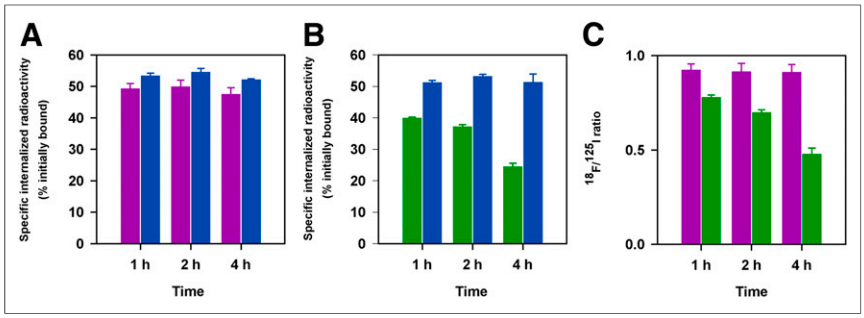

FIGURE 2. Paired-label internalization of ^{125}I-SGMIB-5F7 (blue bars) versus ^{18}F-RL-I-5F7 (magenta bars) (A) and ^{125}I-SGMIB-5F7 (blue bars) versus ^{18}F-SFB-5F7 (green bars) (B) in BT-471M1 breast cancer cells in vitro. (C) Ratio of ^{18}F to ^{125}I obtained from 2 experiments.

2 experiments, and the resultant ^{18}F-to-^{125}I ratios shown in Figure 2C further demonstrate the advantage of ^{18}F-RL-I-5F7 over ^{18}F-SFB-5F7 with regard to intracellular trapping of ^{18}F activity. These results suggest that RL-I, like SGMIB, helps retain radioactivity in BT474M1 cells in vitro after internalization of labeled Nanobody.

Biodistribution Studies

The tissue distribution of ^{18}F-RL-I-5F7 and ^{18}F-SFB-5F7 were compared with that of coadministered ^{125}I-SGMIB-5F7 in mice with BT474M1 xenografts at 1 and 2 h, and the results are presented in Tables 1 and 2, respectively. Tumor uptake of ^{18}F-RL-I-5F7 increased from 29.0 ± 3.9 %ID/g at 1 h to 36.3 ± 14.1 %ID/g at 2 h and was significantly higher ($P < 0.05$) than that of coadministered ^{125}I-SGMIB-5F7. In contrast, tumor uptake of ^{18}F-SFB-5F7 was also more than 20 %ID/g but significantly lower ($P < 0.05$) than that of coadministered ^{125}I-SGMIB-5F7 at all time points. When normalized to ^{125}I-SGMIB-5F7 levels (Fig. 3), the tumor uptake of ^{18}F-RL-I-5F7 was 26%–28% higher ($P < 0.05$) than that of ^{18}F-SFB-5F7, consistent with the hypothesized effects of charged guanidine (*17*) and polar triazole (*21*) moieties in ^{18}F-RL-I on trapping of labeled catabolites, thereby enhancing tumor uptake. Generally, uptake of the 2 ^{18}F-5F7 conjugates in normal tissues was more than an order of magnitude lower than that in tumor, with the exception of renal levels for ^{18}F-RL-I-5F7, which were comparable to those for ^{125}I-SGMIB-5F7. Tumor–to–normal-tissue ratios for both ^{18}F-labeled 5F7 conjugates increased from 1 to 2 h after injection (Fig. 4). With ^{18}F-RL-I-5F7, the tumor-to-blood and tumor-to-muscle ratios at 2 h reached 47 ± 13 and 38 ± 21, respectively, values that were higher than those observed for ^{18}F-SFB-5F7 (25 ± 10; $P < 0.02$ and 30 ± 17; $P > 0.05$, respectively). In contrast, tumor-to-tissue ratios for ^{18}F-SFB-5F7 were higher than those for ^{18}F-RL-I-5F7 in the liver, spleen, bone, and most notably, kidneys ($P < 0.04$–0.001).

Small-Animal PET/CT Imaging

Representative small-animal PET/CT whole-body coronal images of the mice with BT474M1 xenografts obtained 1 and 2 h after injection of ^{18}F-RL-I-5F7 as well as for a mouse receiving a blocking dose of trastuzumab 24 h before tracer injection are shown in Figure 5. SUV and %ID/g values calculated from the imaging data are presented in Table 3; consistent with the necropsy experiments, high tumor uptake was observed at both time

TABLE 1
Paired-Label Biodistribution of ^{18}F-RL-I-5F7 and ^{125}I-SGMIB-5F7 in Severe Combined Immunodeficiency Mice Bearing BT474M1 Xenografts

	%ID/g*			
	1 h		2 h	
Tissue	^{125}I-SGMIB	^{18}F-RL-I-5F7	^{125}I-SGMIB	^{18}F-RL-I-5F7
Liver	3.27 ± 0.61	3.42 ± 0.57†	3.12 ± 0.94	3.17 ± 1.13†
Spleen	2.01 ± 0.62	1.63 ± 0.51	1.85 ± 0.49	1.31 ± 0.40
Lung	10.47 ± 2.27	9.07 ± 1.06†	8.03 ± 0.83	6.63 ± 1.46†
Heart	1.43 ± 0.47	1.30 ± 0.53†	0.62 ± 0.15	0.54 ± 0.14†
Kidney	122.68 ± 18.03	139.45 ± 20.54	96.92 ± 30.55	105.02 ± 39.52†
Stomach	1.91 ± 0.77	1.97 ± 0.78†	0.59 ± 0.28	0.54 ± 0.23†
Small intestine	1.71 ± 0.52	2.10 ± 0.59	0.94 ± 0.30	1.28 ± 0.42
Large intestine	1.36 ± 0.31	1.68 ± 0.37	1.89 ± 1.30	2.47 ± 1.63
Muscle	1.16 ± 0.48	1.27 ± 0.50	0.91 ± 0.30	1.10 ± 0.38†
Blood	1.75 ± 0.84	1.95 ± 0.87	0.65 ± 0.41	0.83 ± 0.43
Bone	0.76 ± 0.37	0.97 ± 0.31	0.78 ± 0.23	1.13 ± 0.28
Brain	0.10 ± 0.04	0.11 ± 0.04	0.07 ± 0.01	0.07 ± 0.02†
Tumor	26.36 ± 3.12	28.97 ± 3.88	32.52 ± 12.11	36.28 ± 14.10

*Mean ± SD ($n = 5$).
†Difference in uptake not statistically significant.

TABLE 2
Paired Label Biodistribution of ^{18}F-SFB-5F7 and ^{125}I-SGMIB-5F7 in Severe Combined Immunodeficiency Mice Bearing BT474M1 Xenografts

Tissue	%ID/g*			
	1 h		2 h	
	^{125}I-SGMIB	^{18}F-SFB	^{125}I-SGMIB	^{18}F-SFB
Liver	2.02 ± 0.47	0.95 ± 0.21	2.18 ± 0.55	0.68 ± 0.13
Spleen	1.08 ± 0.33	0.67 ± 0.37	1.28 ± 0.22	0.52 ± 0.13
Lung	2.96 ± 0.39	2.31 ± 0.40	2.56 ± 0.70	2.00 ± 0.38†
Heart	0.76 ± 0.20	0.62 ± 0.15	0.62 ± 0.13	0.54 ± 0.15†
Kidney	102.50 ± 26.35	3.90 ± 1.13	93.00 ± 18.82	2.90 ± 0.77
Stomach	1.32 ± 1.17	1.43 ± 1.69†	1.98 ± 1.12	3.21 ± 4.62†
Small intestine	1.17 ± 0.55	0.69 ± 0.33	1.32 ± 0.46	0.59 ± 0.19
Large intestine	1.18 ± 0.47	0.69 ± 0.50	3.86 ± 5.47	1.22 ± 1.66†
Muscle	1.14 ± 0.27	1.16 ± 0.37†	1.21 ± 0.89	1.43 ± 1.20†
Blood	0.96 ± 0.26	1.25 ± 0.29	0.67 ± 0.51	1.44 ± 0.88
Bone	0.88 ± 0.36	0.97 ± 0.55†	0.51 ± 0.09	0.54 ± 0.08†
Brain	0.07 ± 0.02	0.09 ± 0.02	0.08 ± 0.05	0.12 ± 0.06
Tumor	27.88 ± 8.08	23.94 ± 7.00	33.59 ± 6.24	29.59 ± 5.10

*Mean ± SD (n = 5).
†Difference in uptake not statistically significant.

points. No significant uptake was seen in normal organs other than the kidneys and bladder, resulting in high-contrast images. Preinjection of trastuzumab reduced tumor accumulation of ^{18}F-RL-I-5F7 by more than 90%, confirming that tumor localization was HER2-specific.

DISCUSSION

Nanobodies are an attractive platform for use in tandem with short-lived positron emitters because of their rapid tumor uptake and normal-tissue clearance (*15*). A recent phase-1 clinical study with a ^{68}Ga-labeled Nanobody (^{68}Ga-NOTA-2Rs15 d) demonstrated the feasibility of evaluating HER2 status in patients with breast carcinoma metastases by immuno-PET (*22*). Although encouraging results were reported, ^{18}F might be an even more attractive radionuclide for labeling Nanobodies for several reasons. Compared with ^{68}Ga, ^{18}F has a more than 3-fold-lower energy and tissue range, resulting in improved spatial resolution. Moreover, the longer physical half-life of ^{18}F provides the option for delayed imaging in circumstances in which background activity may be problematic and also allows radiopharmaceutical distribution from regional production sites, facilitating widespread use. In the present study, we have evaluated 2 approaches for labeling Nanobodies with ^{18}F—a novel residualizing label that we developed for ^{18}F labeling of proteins and peptides targeting internalizing receptors such as HER2 (*17*) as well as ^{18}F-SFB, the most widely used protein/peptide radiofluorination agent for which several automated procedures have already been developed (*23*).

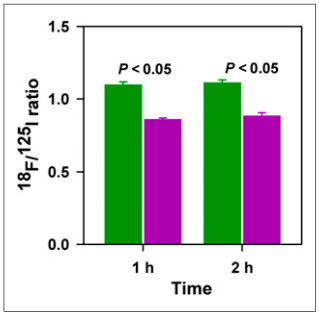

FIGURE 3. ^{18}F-to-^{125}I ratio in tumor from paired-label biodistribution of ^{18}F-RL-I5F7 and ^{125}I-SGMIB-5F7 and ^{18}F-SFB-5F7 and ^{125}I-SGMIB-5F7 in severe combined immunodeficiency mice bearing BT474M1 xenografts. Green bars = ^{18}F-RL-I-5F7; magenta bars = ^{18}F-SFB-5F7.

Our previous studies with radioiodinated anti-HER2 5F7 Nanobody documented the importance of using a residualizing labeling approach for maximizing retention of radioactivity in HER2-expressing tumors (*16,19*). Because peak and cumulative tumor radioactivity levels with ^{131}I-SGMIB-5F7 were considerably higher than previously reported for any Nanobody radionuclide combination (*15*), SGMIB was selected as the design template for creating an ^{18}F-labeled residualizing label. ^{18}F-RL-I was synthesized and used to label the 5F7 Nanobody in reasonable radiochemical yield, with preservation of immunoreactivity (62%–80%) and affinity (4.7 ± 0.9 nM) for HER2 after labeling (*17*).

The potential advantage of the residualizing labeling agent was first evaluated in internalization assays performed with HER2-expressing BT474M1 breast carcinoma cells. Because there is no suitable fluorine radionuclide to use in tandem with ^{18}F, direct paired-label comparisons of Nanobody labeled with ^{18}F-RL-I and ^{18}F-SFB cannot be performed. Instead, indirect comparison was made by performing 2 paired-label studies with ^{125}I-SGMIB-5F7 serving as a common reference. Intracellularly trapped radioactivity levels for 5F7 labeled with ^{18}F-RL-I remained constant at more than 47% of initial cell-bound radioactivity over the 4-h experiment and were similar to those for coincubated ^{125}I-SGMIB-5F7. In contrast, intracellular radioactivity levels for ^{18}F-SFB-5F7 were lower and

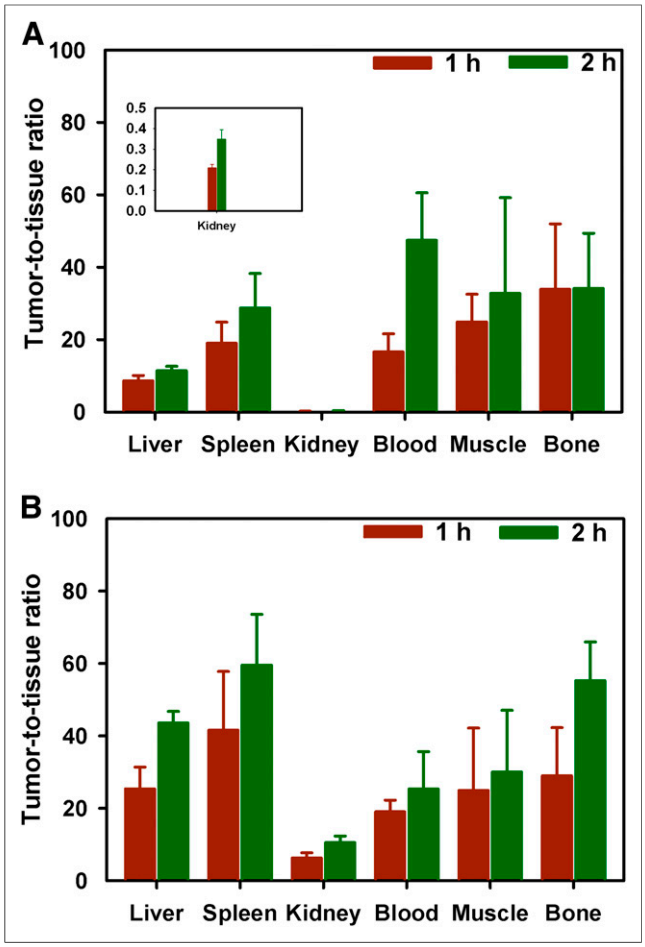

FIGURE 4. Tumor-to-tissue ratios for selected tissues obtained from biodistribution of ^{18}F-RL-I-5F7 (A) and ^{18}F-SFB-5F7 (B).

decreased with time, and exhibited behavior on this cell line similar to 5F7-GGC Nanobody labeled using IODO-GEN (*16*), demonstrating the residualizing capability of the ^{18}F-RL-I moiety.

Biodistribution and small-animal PET imaging experiments in severe combined immunodeficiency mice with HER2-expressing BT474M1 xenografts demonstrated rapid tumor accumulation and blood-pool clearance of ^{18}F-RL-I-5F7. Pretreatment with trastuzumab reduced tumor levels more than 10-fold, confirming that uptake was HER2-specific. When normalized to coadministered ^{125}I-SGMIB-5F7, tumor accumulation of ^{18}F-RL-I-5F7 was 26%–28% higher than that observed with ^{18}F-SFB-5F7 at 1 and 2 h, consistent with the 16%–24% higher normalized intracellular activity measured with BT474M1 cells in vitro for ^{18}F-RL-I-5F7. By 4 h, the intracellular retention advantage increased to 47%, suggesting that the residualizing ability of the RL-I prosthetic group might be even more pronounced in vivo at later time points.

It is worth noting that the tumor accumulation of 5F7 after labeling with both ^{18}F-labeled prosthetic groups was higher than that observed in this xenograft model when this Nanobody was radioiodinated using either the IODO-GEN or the IB-Mal-D-GEEEK methods (*16,19*) and considerably higher than that reported for any other combination of Nanobody, radionuclide, and xenograft model (*15,24,25*). With regard to other studies with ^{18}F, tumor accumulation of Nanobodies labeled using ^{18}F-SFB and targeting the macrophage mannose receptor (*26*) and HER2 (*27*) were reported to be 2.40 ± 0.46 %ID/g (3 h) and 3.09 ± 0.02 %ID/g (1 h), respectively, about 10-fold lower than observed in the current study. Use of a sortase-based site-specific method involving a click reaction for labeling Nanobodies with ^{18}F also has been reported (*28*); however, the goal was imaging immune response to tumor, not a cancer cell surface molecular target.

It is also relevant to compare the tumor targeting of these ^{18}F-labeled 5F7 conjugates with ^{18}F-labeled anti-HER2 Affibody molecules because of the similarity in molecular weight (6.5 vs. 12–15 kDa) and intended clinical application for these labeled proteins. In studies with HER2-specific $Z_{HER2:342}$ Affibody labeled via *N*-2-(4-^{18}F-fluorobenzamido)ethyl]maleimide performed in mice with xenografts expressing high levels of HER2, peak tumor uptake occurred at 1 h and ranged from about 10–22 %ID/g (*29,30*). A second-generation Affibody, $Z_{HER2:2891}$ (GE-226) with improved HER2 affinity (76 pM), was evaluated in mice with HER2-expressing NCI-N87 xenografts after labeling with ^{18}F by 3 methods; optimal tumor accumulation was obtained (7.15 ± 0.69 %ID/g at 90 min) when labeling was performed using 4-^{18}F-fluorobenzaldehyde (FBA) (*31*). In a subsequent PET imaging study with ^{18}F-FBA-GE-226, peak tumor uptake in 3 high-HER2-expressing xenografts ranged from 10.9 ± 1.5 %ID/mL for MCF7-HER2 to 18.7 ± 2.4 %ID/mL for SKOV-3 (*14*). Although differences in variables such as animal model, protein dose, and internalization rate could play a role (*32*), the results obtained in the current study with ^{18}F-labeled anti-HER2 5F7 Nanobody compare favorably with those reported for ^{18}F-labeled Affibody molecules.

Normal-tissue clearance of the labeled Nanobody conjugates was quite rapid except from the kidneys for ^{18}F-RL-I-5F7 and ^{125}I-SGMIB-5F7. This behavior is consistent with the high degree of renal retention observed with other proteins with molecular weights less than 60 kDa (*33*) as well as Nanobodies labeled with radiometals (*15*), other residualizing radiohalgen moieties (*19*), and those containing polar amino acid residues at the C-terminal (*24,25*). Exceptions to this behavior are Nanobodies labeled with radioiodine using IODO-GEN (*16,19*), presumably reflecting their rapid dehalogenation in vivo and the about 30-fold-lower kidney uptake observed in the current study for ^{18}F-SFB-5F7, compared

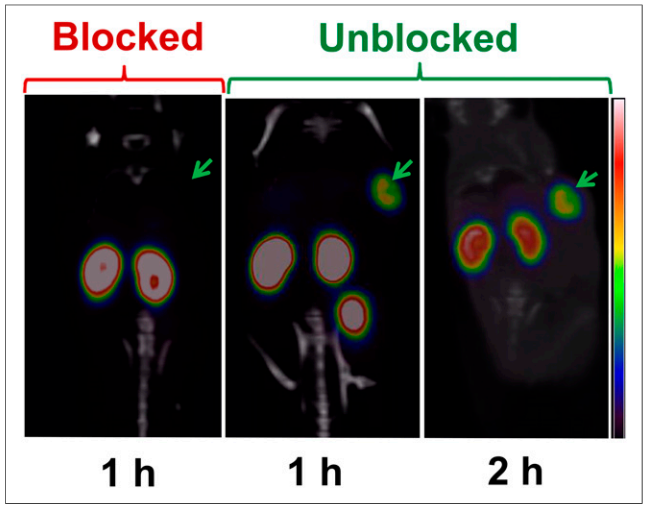

FIGURE 5. PET/CT images of mice bearing BT474M1 xenografts after injection of ^{18}F-RL-I-5F7. Images were obtained at 1 and 2 h without and at 1 h with blocking of HER2 receptors by preadministration of trastuzumab.

TABLE 3
Tumor SUV and %ID/g from Small-Animal PET/CT Imaging of Severe Combined Immunodeficiency Mice Bearing BT474M1 Xenografts after Injection of ^{18}F-RL-I-5F7

	1 h		2 h	
Mouse no.	SUV	%ID/g	SUV	%ID/g
Unblocked				
1*	4.2 ± 0.7	22.4 ± 3.8	4.3 ± 0.8	23.0 ± 4.2
2*	3.3 ± 0.4	17.8 ± 2.1	3.6 ± 0.7	19.4 ± 4.1
3†	4.9 ± 0.7	26.4 ± 3.9	4.9 ± 0.8	26.2 ± 4.2
4†	4.4 ± 0.6	24.9 ± 3.3	4.6 ± 0.7	26.1 ± 3.7
Blocked				
1*	0.4 ± 0.1	2.1 ± 0.1	ND	ND
2*	0.4 ± 0.1	2.1 ± 0.8	ND	ND
3†	0.3 ± 0.1	1.3 ± 0.5	ND	ND
4†	0.2 ± 0.1	1.0 ± 0.5	ND	ND

*Batch1.
†Batch2.
ND = not determined.

with ^{18}F-RL-I-5F7 and ^{125}I-SGMIB-5F7. A factor that could contribute to the low renal activity levels seen with ^{18}F-SFB-5F7 is the formation of 4-^{18}F-fluorohippuric acid, the primary metabolite reported from other proteins labeled using the ^{18}F-SFB method (*34*). On the other hand, the polar triazole (*21*) and especially the guanidine moieties in ^{18}F-RL-I might have contributed to its high renal retention as seen with Nanobodies bearing other polar functionalities (*24,25*). Future studies are planned to determine whether the radioactivity retained in the kidneys is due to intact ^{18}F-RL-I-5F7 or trapping of lower-molecular-weight catabolites generated by its lysosomal proteolysis (*33,35*).

From an imaging perspective, high renal activity levels should not interfere with lesion detection both for primary and the most common sites of metastases for HER2-positive cancers, as was demonstrated in a recent study with a ^{68}Ga-NOTA anti-HER2 Nanobody (*22*). If necessary, a significant reduction in kidney uptake of radiolabeled Nanobodies can be achieved through the use of positively charged amino acids or the plasma expander Gelofusine (Braun Medical) (*24*). It also may be possible to decrease kidney uptake by introducing brush border enzyme-cleavable linkers in the prosthetic moiety (*35,36*), and efforts in this direction are under way in our laboratories. In addition, these ^{18}F-labeled 5F7 conjugates are not retained in the liver, a frequent site of metastases for HER2-positive breast cancers. This is a potential advantage compared with other HER2-specific immuno-PET agents such as ^{89}Zr-DFO-trastuzumab that exhibit significant accumulation in the liver (*37*).

CONCLUSION

The results of this study demonstrate the feasibility of using ^{18}F-labeled anti-HER2 Nanobodies for the evaluation of HER2-expressing cancers. Excellent tumor targeting was observed with both reagents; however, use of the recently developed residualizing agent ^{18}F-RL-I resulted accumulation and retention of significantly higher ^{18}F levels in BT474M1 human breast carcinoma cells and xenografts compared with ^{18}F-SFB. As has been observed previously with Nanobodies labeled with residualizing radiometals, renal uptake of ^{18}F-RL-I-5F7 was high, which if problematic, might require compensatory strategies such as Gelofusine administration. Both ^{18}F-RL-I-5F7 and ^{18}F-SFB-5F7 warrant further evaluation as tracers for the evaluation of HER2-expressing cancers using immuno-PET.

DISCLOSURE

The costs of publication of this article were defrayed in part by the payment of page charges. Therefore, and solely to indicate this fact, this article is hereby marked "advertisement" in accordance with 18 USC section 1734. This work was supported in part by National Institutes of Health grants CA188177 and CA42324 and for small-animal PET imaging, by S10RR31792. No other potential conflict of interest relevant to this article was reported.

ACKNOWLEDGMENTS

We thank Hilde Revets (Ablynx, Belgium) for providing the 5F7 Nanobody, Xiao-Guang Zhao for biodistribution studies, and Thomas Hawk for help with small-animal PET imaging studies.

REFERENCES

1. DeSantis CE, Lin CC, Mariotto AB, et al. Cancer treatment and survivorship statistics, 2014. *CA Cancer J Clin.* 2014;64:252–271.
2. Howlader N, Chen VW, Ries LA, et al. Overview of breast cancer collaborative stage data items: their definitions, quality, usage, and clinical implications: a review of SEER data for 2004-2010. *Cancer.* 2014;120(suppl 23): 3771–3780.
3. Nielsen DL, Kumler I, Palshof JA, Andersson M. Efficacy of HER2-targeted therapy in metastatic breast cancer: monoclonal antibodies and tyrosine kinase inhibitors. *Breast.* 2013;22:1–12.
4. Zeglinski M, Ludke A, Jassal DS, Singal PK. Trastuzumab-induced cardiac dysfunction: a 'dual-hit'. *Exp Clin Cardiol.* 2011;16:70–74.
5. Wolff AC, Hammond ME, Hicks DG, et al. Recommendations for human epidermal growth factor receptor 2 testing in breast cancer: American Society of Clinical Oncology/College of American Pathologists Clinical Practice Guideline Update. *J Clin Oncol.* 2013;31:3997–4013.
6. Molina R, Barak V, van Dalen A, et al. Tumor markers in breast cancer: European Group on Tumor Markers recommendations. *Tumour Biol.* 2005; 26:281–293.
7. Minot DM, Voss J, Rademacher S, et al. Image analysis of HER2 immunohistochemical staining: reproducibility and concordance with fluorescence in situ hybridization of a laboratory-validated scoring technique. *Am J Clin Pathol.* 2012;137:270–276.
8. Fabi A, Di Benedetto A, Metro G, et al. HER2 protein and gene variation between primary and metastatic breast cancer: significance and impact on patient care. *Clin Cancer Res.* 2011;17:2055–2064.
9. Sapino A, Goia M, Recupero D, Marchio C. Current challenges for HER2 testing in diagnostic pathology: state of the art and controversial issues. *Front Oncol.* 2013;3:129.
10. Zidan J, Dashkovsky I, Stayerman C, Basher W, Cozacov C, Hadary A. Comparison of HER-2 overexpression in primary breast cancer and metastatic sites and its effect on biological targeting therapy of metastatic disease. *Br J Cancer.* 2005;93:552–556.
11. Cardoso F, Costa A, Norton L, et al. ESO-ESMO 2nd international consensus guidelines for advanced breast cancer (ABC2). *Breast.* 2014;23:489–502.
12. Mortimer JE, Bading JR, Colcher DM, et al. Functional imaging of human epidermal growth factor receptor 2-positive metastatic breast cancer using ^{64}Cu-DOTA-trastuzumab PET. *J Nucl Med.* 2014;55:23–29.
13. Olafsen T, Sirk SJ, Olma S, Shen CK, Wu AM. ImmunoPET using engineered antibody fragments: fluorine-18 labeled diabodies for same-day imaging. *Tumour Biol.* 2012;33:669–677.
14. Trousil S, Hoppmann S, Nguyen QD, et al. Positron emission tomography imaging with ^{18}F-labeled ZHER2:2891 affibody for detection of HER2 expression and pharmacodynamic response to HER2-modulating therapies. *Clin Cancer Res.* 2014;20:1632–1643.

15. D'Huyvetter M, Xavier C, Caveliers V, Lahoutte T, Muyldermans S, Devoogdt N. Radiolabeled nanobodies as theranostic tools in targeted radionuclide therapy of cancer. *Expert Opin Drug Deliv.* 2014;11:1939–1954.
16. Pruszynski M, Koumarianou E, Vaidyanathan G, et al. Improved tumor targeting of anti-HER2 nanobody through *N*-succinimidyl 4-guanidinomethyl-3-iodobenzoate radiolabeling. *J Nucl Med.* 2014;55:650–656.
17. Vaidyanathan G, McDougald D, Choi J, et al. *N*-succinimidyl 3-((4-(4-[^{18}F] fluorobutyl)-^{1}H-1,2,3-triazol-1-yl)methyl)-5-(guanidinomethyl)benzoate ([^{18}F] SFBTMGMB): a residualizing label for ^{18}F-labeling of internalizing biomolecules. *Org Biomol Chem.* 2016;14:1261–1271.
18. Vaidyanathan G, Zalutsky MR. Synthesis of *N*-succinimidyl 4-[^{18}F]fluorobenzoate, an agent for labeling proteins and peptides with ^{18}F. *Nat Protoc.* 2006;1:1655–1661.
19. Pruszynski M, Koumarianou E, Vaidyanathan G, et al. Targeting breast carcinoma with radioiodinated anti-HER2 nanobody. *Nucl Med Biol.* 2013;40:52–59.
20. Yu Z, Xia W, Wang HY, et al. Antitumor activity of an Ets protein, PEA3, in breast cancer cell lines MDA-MB-361DYT2 and BT474M1. *Mol Carcinog.* 2006;45:667–675.
21. Waldmann CM, Hermann S, Faust A, et al. Novel fluorine-18 labeled 5-(1-pyrrolidinylsulfonyl)-7-azaisatin derivatives as potential PET tracers for in vivo imaging of activated caspases in apoptosis. *Bioorg Med Chem.* 2015;23:5734–5739.
22. Keyaerts M, Xavier C, Heemskerk J, et al. Phase I study of ^{68}Ga-HER2-Nanobody for PET/CT assessment of HER2-expression in breast carcinoma. *J Nucl Med.* 2016;57:27–33.
23. Richter S, Wuest F. ^{18}F-Labeled peptides: the future is bright. *Molecules.* 2014;19:20536–20556.
24. D'Huyvetter M, Vincke C, Xavier C, et al. Targeted radionuclide therapy with a ^{177}Lu-labeled anti-HER2 nanobody. *Theranostics.* 2014;4:708–720.
25. Xavier C, Vaneycken I, D'Huyvetter M, et al. Synthesis, preclinical validation, dosimetry, and toxicity of ^{68}Ga-NOTA-anti-HER2 nanobodies for iPET imaging of HER2 receptor expression in cancer. *J Nucl Med.* 2013;54:776–784.
26. Blykers A, Schoonooghe S, Xavier C, et al. PET Imaging of macrophage mannose receptor-expressing macrophages in tumor stroma using ^{18}F-radiolabeled camelid single-domain antibody fragments. *J Nucl Med.* 2015;56:1265–1271.
27. Vaneycken I, Xavier C, Blykers A, Devoogdt B, Caveliers V, Lahoutte T. Synthesis and first in vivo evaluation of ^{18}F-anti-HER2-nanobodies: a new probe for PET imaging of HER2 expression in breast cancer [abstract]. *J Nucl Med.* 2011;52:664–665.
28. Rashidian M, Keliher EJ, Bilate AM, et al. Noninvasive imaging of immune responses. *Proc Natl Acad Sci USA.* 2015;112:6146–6151.
29. Kramer-Marek G, Kiesewetter DO, Capala J. Changes in HER2 expression in breast cancer xenografts after therapy can be quantified using PET and ^{18}F-labeled affibody molecules. *J Nucl Med.* 2009;50:1131–1139.
30. Kramer-Marek G, Kiesewetter DO, Martiniova L, Jagoda E, Lee SB, Capala J. [^{18}F]FBEM-Z(HER2:342)-affibody molecule-a new molecular tracer for in vivo monitoring of HER2 expression by positron emission tomography. *Eur J Nucl Med Mol Imaging.* 2008;35:1008–1018.
31. Glaser M, Iveson P, Hoppmann S, et al. Three methods for ^{18}F labeling of the HER2-binding affibody molecule $Z_{HER2:2891}$ including preclinical assessment. *J Nucl Med.* 2013;54:1981–1988.
32. Malmberg J, Sandström M, Wester K, Tolmachev V, Orlova A. Comparative biodistribution of imaging agents for in vivo molecular profiling of disseminated prostate cancer in mice bearing prostate cancer xenografts: focus on ^{111}In- and ^{125}I-labeled anti-HER2 humanized monoclonal trastuzumab and ABY-025 affibody. *Nucl Med Biol.* 2011;38:1093–1102.
33. Akizawa H, Uehara T, Arano Y. Renal uptake and metabolism of radiopharmaceuticals derived from peptides and proteins. *Adv Drug Deliv Rev.* 2008;60:1319–1328.
34. Pietzsch J, Bergmann R, Wuest F, Pawelke B, Hultsch C, van den Hoff J. Catabolism of native and oxidized low density lipoproteins: in vivo insights from small animal positron emission tomography studies. *Amino Acids.* 2005;29:389–404.
35. Akizawa H, Imajima M, Hanaoka H, Uehara T, Satake S, Arano Y. Renal brush border enzyme-cleavable linkages for low renal radioactivity levels of radiolabeled antibody fragments. *Bioconjug Chem.* 2013;24:291–299.
36. Li L, Olafsen T, Anderson AL, Wu A, Raubitschek AA, Shively JE. Reduction of kidney uptake in radiometal labeled peptide linkers conjugated to recombinant antibody fragments: site-specific conjugation of DOTA-peptides to a Cys-diabody. *Bioconjug Chem.* 2002;13:985–995.
37. Dijkers EC, Oude Munnink TH, Kosterink JG, et al. Biodistribution of ^{89}Zr-trastuzumab and PET imaging of HER2-positive lesions in patients with metastatic breast cancer. *Clin Pharmacol Ther.* 2010;87:586–592.